Molecular Mechanism of Distinct Salt-Dependent Enzyme Activity of Two Halophilic Nucleoside Diphosphate Kinases

Akihiro Yamamura,[†] Takefumi Ichimura,[†] Masahiro Kamekura,[‡] Toru Mizuki,[§] Ron Usami,[§] Tsukasa Makino,[†] Jun Ohtsuka,[†] Ken-ichi Miyazono,[†] Masahiko Okai,[†] Koji Nagata,[†] and Masaru Tanokura[†]*

[†]Department of Applied Biological Chemistry, Graduate School of Agricultural and Life Sciences, University of Tokyo, Bunkyo-ku, Tokyo 113-8657, Japan; [‡]Noda Institute for Scientific Research, Noda-shi, Chiba 278-0037, Japan; and [§]Bio-Nano Electronics Research Centre, Toyo University, Kawagoe-shi, Saitama 350-8585, Japan

ABSTRACT Nucleoside diphosphate kinases from haloarchaea *Haloarcula quadrata* (NDK-q) and *H. sinaiiensis* (NDK-s) are identical except for one out of 154 residues, i.e., Arg^{31} in NDK-q and Cys^{31} in NDK-s. However, the salt-dependent activity profiles of NDK-q and NDK-s are quite different: the optimal NaCl concentrations of NDK-q and NDK-s are 1 M and 2 M, respectively. We analyzed the relationships of the secondary, tertiary, and quaternary structures and NDK activity of these NDKs at various salt concentrations, and revealed that 1), NDK-q is present as a hexamer under a wide range of salt concentrations (0.2–4 M NaCl), whereas NDK-s is present as a hexamer at an NaCl concentration above 2 M and as a dimer at NaCl concentrations below 1 M; 2), dimeric NDK-s has lower activity than hexameric NDK-s; and 3), dimeric NDK-s has higher helicity than hexameric NDK-s. We also determined the crystal structure of hexameric NDK-q, and revealed that Arg^{31} plays an important role in stabilizing the hexamer. Thus the substitution of Arg (as in NDK-q) to Cys (as in NDK-s) at position 31 destabilizes the hexameric assembly, and causes dissociation to less active dimers at low salt concentrations.

INTRODUCTION

Nucleoside diphosphate kinase (NDK), which is ~150 residues long, is an enzyme with a main function of transferring γ-phosphate from a nucleoside triphosphate to a diphosphate, to maintain cellular pools of all nucleoside triphosphates (1). It is an essential enzyme for many living organisms, from archaea through mammals. All NDKs have an $\alpha\beta$ sandwich composed of two $\beta\alpha\beta$ units (also called a ferredoxin fold), a Kpn loop composed of a surface α-helix hairpin, and a C-terminal segment that interacts with the neighboring subunit (2). The NDKs from various sources are present as dimers, trimers, tetramers, or hexamers, or in equilibrium between two of these states (3).

Haloarchaea, which are extremely halophilic aerobic archaea, grow best in the presence of 3.5–4.5 M NaCl, and they accumulate salts, mainly KCl, at concentrations up to 5 M within the cell. Most of the haloarchaeal proteins are thus adapted to function at a high salt concentration, and tend to lose their activities at low salt concentrations (4). The molecular surfaces of all known haloarchaeal enzymes are highly negatively charged, provide hydrated carboxylate groups to maintain the solubility of proteins, and prevent the enhancement of hydrophobic interactions under high salt concentrations (5). Haloarchaeal NDK was first identified in *Natrialba magadii* as a major cytosolic protein that is active over a wide range of salt concentrations (0.09–3.5 M NaCl) (6). Further studies showed that NDKs from halobacteria are one of the few halophilic enzymes with a tolerance to low salt concentrations.

The first crystal structure of halophilic NDK was solved for *Halobacterium salinarum* NDK (7). Its quaternary structure changes, depending on salt concentration: it is a hexamer in 3.8 M NaCl, and a dimer in 0.2 M NaCl. Circular dichroism (CD) analysis showed that the hexamer and dimer possess α-helix contents of 29% and 19%, respectively (8). A single mutation, Gly^{114} to Arg (G114R), stabilizes the hexamer at a low salt concentration of 0.2 M NaCl (9). Gly^{114} is located at the hexameric interface. The distance between Gly^{114} and Glu^{155} in the neighboring subunit is 5.6 Å, and thus Arg^{114} in the G114R mutant interacts electrostatically with Glu^{155} of the neighboring subunit, resulting in the stabilization of the hexamer.

Our recent studies identified nine NDKs from the genus *Haloarcula*, a halobacterium that requires at least 1.5 M NaCl for growth, and 2.0–4.5 M NaCl for optimal growth (10). The amino-acid sequences of the nine *Haloarcula* NDKs are almost the same; they are different at four positions at maximum. The NDKs from *H. quadrata* (NDK-q) and *H. sinaiiensis* (NDK-s) are identical except at position 31, which is Arg^{31} in NDK-q, and Cys^{31} in NDK-s, but their salt-dependent activity profiles are quite different. Both NDK-q and NDK-s are active over a wide range of salt concentrations (0.2–4 M NaCl), but their optimal NaCl concentrations are different, i.e., 1 M and 2 M for NDK-q and NDK-s, respectively.

This study aimed to reveal the structural basis of different salt-dependent activity profiles of NDK-q and NDK-s. We report on the crystal structure of NDK-q at 2.6-Å resolution. We also analyzed the secondary and quaternary structures of of NDK-q and NDK-s, using CD measurements, gel-filtration chromatography, and ultracentrifugation at various NaCl concentrations, and revealed that their different salt-

Submitted December 4, 2008, and accepted for publication March 13, 2009.

*Correspondence: amtanok@mail.ecc.u-tokyo.ac.jp

Editor: Patrick Loria.

0006-3495/09/06/4692/9 $2.00

doi: 10.1016/j.bpj.2009.03.012

dependent activity profiles are mainly the result of different quaternary structures at low salt concentrations.

MATERIALS AND METHODS

Cloning and expression of NDK-q and NDK-s

The genes of NDK-q (GenInfo identifier: 73760118) and NDK-s (GenInfo identifier: 73760116) were amplified by polymerase chain reaction (PCR) by using the *H. quadrata* and *H. sinaiiensis* genomes, respectively, as templates. The PCR primers were 5′-GGAATTCCATATGATGTCCGAG-CACGAGCGC-3′ (including an *Nde*I site) and 5′-CCCAAGCTTTTAT-TACTCGTACAGCCAGGACG-3′ (including a *Hin*dIII site). The PCR products were digested with *Nde*I and *Hin*dIII, and ligated into the T7 expression vector pET-28a(+) (Novagen, Madison, WI). The *Escherichia coli* strain Rosetta (DE3) was used as the host for protein expression. Cells were grown in Lysogeny broth media containing 30 μg/mL kanamycin at 37°C. Cells were induced at an optical density at 600 nm (OD_{600}) of 0.6 with 0.1 mM Isopropyl β-D-1-thiogalactopyranoside during 16 h at 25°C to express N-terminal (6 × His)-tagged NDKs. In recombinant NDK-q and NDK-s, the N-terminal Met, which is eliminated in native NDK-q and NDK-s, is added to the amino-acid sequence as Met^1. Thus the residue numbers are different from those in our previous report (10).

Purification of NDKs

Harvested cells were resuspended in 50 mM Tris-HCl (pH 8.0), 2 mM $MgCl_2$, 40 mM imidazole, and 2 M NaCl, and then disrupted by sonication. The lysate was centrifuged at 40,000 × *g* at 4°C for 30 min, and the resulting supernatant was loaded onto an Ni Sepharose 6 Fast Flow (GE Healthcare Biosciences, Uppsala, Sweden) column equilibrated with the same buffer. The column was washed with the same buffer to remove nonspecifically bound protein, and then the protein was eluted with a stepwise gradient of 40 to 200 mM imidazole. The protein was concentrated to 5 mg/mL using 20-mL Vivaspin concentrator (5-kDa cutoff size; Sartorius, Germany), and then applied to a Superdex 200 HR 10/30 column (GE Healthcare Biosciences) equilibrated with 50 mM Tris-HCl (pH 8.0), 2 mM $MgCl_2$, and 2 M NaCl. Then the purified protein was concentrated to 10 mg/mL, using 20-mL Vivaspin concentrator (5-kDa cutoff size; Sartorius).

Crystallization and data collection

The sitting drop vapor diffusion method was used for crystallization. Purified NDK-q solution (10 mg/mL) and reservoir solution, 0.7 μL each, were mixed to prepare a crystallization drop, and the drop was equilibrated against 500 μL of reservoir solution. Crystals of NDK-q were grown at 20°C with a reservoir solution of 100 mM HEPES-NaOH buffer (pH 7.6), 18% (w/v) PEG 400, and 10 mM EDTA. Crystals grew to a final dimension of 0.2 × 0.2 × 0.3 mm^3 within 1 day. Crystals were picked up with mounting loops, transferred into another drop consisting of 100 mM HEPES-NaOH buffer (pH 7.6), 25% (w/v) PEG 400, and 10 mM EDTA, and frozen directly in liquid nitrogen, using 25% PEG 400 as cryoprotectant. The x-ray diffraction data of NDK-q crystals were obtained at beamline NW12 at Photon Factory-Advanced Ring (PF-AR) (High Energy Accelerator Research Organization, Tsukuba, Japan). The best crystal diffracted to a 2.6-Å resolution, and belonged to the space group $P6_3$, with unit cell dimensions $a = 73.57$ Å, $b = 73.57$ Å, and $c = 214.27$ Å.

Structure solution and refinement

The x-ray diffraction data were processed with the program package HKL2000 (11) and the CCP4 suite (12). The initial structure was obtained by the molecular replacement method, using the program Molrep (13) in the CCP4 suite. Our search model was the crystal structure of NDK from *Bovine retina* (Protein Data Bank code 1BHN). The initial structure was refined using Xfit (14), CNS (15), and Refmac5 (16) in the CCP4 suite. The stereochemistry of the structure was checked by the program PROCHECK (17). The coordinates and structure factors of the NDK-q structure were deposited in the Protein Data Bank (PDB) as 2ZUA.

Structure comparison

Comparisons between the structure of NDK-q and related structures were performed by superposing two structures, using DaliLite (Cambridge, United Kingdom) (18).

Preparation of NDK-q and NDK-s at various NaCl concentrations

The purified NDK-q and NDK-s in 50 mM Tris-HCl (pH 8.0), 2 mM $MgCl_2$, and 2 M NaCl at a concentration of 10 mg/mL were diluted to 1 or 0.2 mg/mL by adding 50 mM Tris-HCl (pH 8.0) and 2 mM $MgCl_2$ containing appropriate concentrations of NaCl, to adjust the final NaCl concentrations to 0.2, 0.5, 1, 2, 3, or 4 M NaCl, followed by incubation for 1 day at 4°C.

Preparation of dimeric NDK-s at 2 M NaCl

The purified NDK-s in 50 mM Tris-HCl (pH 8.0), 2 mM $MgCl_2$, and 2 M NaCl at a concentration of 10 mg/mL was diluted to 2.5 mg/mL by adding 50 mM Tris-HCl (pH 8.0) and 2 mM $MgCl_2$, to adjust the final NaCl concentration to 0.5 M. After incubation for 1 day at 4°C, the protein was diluted to 0.5 mg/mL by adding 50 mM Tris-HCl (pH 8.0), 2 mM $MgCl_2$, and 2.375 M NaCl, to adjust the NaCl concentration to 2 M. One milliliter of the solution was applied to a Superdex 200 HR 10/30 column (GE Healthcare Biosciences) equilibrated with 50 mM Tris-HCl (pH 8.0), 2 mM $MgCl_2$, and 2 M NaCl, and the fraction containing dimeric NDK-s at an elution volume of 16.5 mL was collected.

Activity assay

The NDK activity was measured using GTP and ADP as substrates, as described previously (10). The amount of ATP produced was determined by a luciferase assay and read in a Lumitester K-210 luminometer (Kikkoman Corp., Noda, Japan). The reaction mixture contained 1.0 mM GTP, 0.5 mM ADP, and 25 mM $MgCl_2$ in 50 mM Tris-HCl (pH 8.0) containing 0, 1, 2, 3, or 4 M NaCl. Three microliters of NDK-q and NDK-s, diluted appropriately, were added to 97 μL of the reaction mixture, and incubated at 37°C. After 1 min and 10 min of incubation, 1 μL of aliquot was taken for the luciferase assay. The luciferin-luciferase reaction was performed in a microtube specially designed for the Lumitester, to which 600 μL of a substrate mixture solution containing 86 μL D-luciferin, 5 mM $MgCl_2$, and 25 mM Tris-HCl (pH 8.0) were added. One microliter of NaCl solution (at 4, 3, 2, 1, and 0 M, to compensate for NaCl in the reaction mixture) was added to the substrate mix. Then 15 μL of luciferase solution (Sigma, St. Louis, MO) were added to the substrate mix, and within 20 s, the NDK reaction product was added to measure the relative luminescence (RLU). The increase in RLU after a 10-min incubation was used as the amount of ATP produced by NDK. The relative activity was calculated from the amount of ATP produced by NDK, where the amount of ATP produced by NDK-q at 1 M NaCl was defined as 100%.

Analytical gel filtration

A hundred microliters of 1 mg/mL NDK-q and NDK-s solutions, dissolved in 0.2, 0.5, 1, 2, 3, or 4 M NaCl in 50 mM Tris-HCl (pH 8.0) and 2 mM $MgCl_2$, were loaded onto a Superdex 200 HR 10/30 column (GE Healthcare Biosciences) and eluted with the same buffer, at a flow rate of 0.5 mL/min at room temperature. The molecular weights of the peaks were calculated from the elution volumes of the standard proteins. Two different protein concentrations (1 and 0.2 mg/mL) were used to examine the effect of protein concentration on the oligomeric state.

Analytical ultracentrifugation

Sedimentation velocity experiments were performed using an Optima XL-I analytical ultracentrifuge (Beckman-Coulter, Fullerton, CA), with a four-hole An60Ti rotor at 20°C. The samples subjected to analytical ultracentrifugation were of 1 mg/mL NDK-q and NDK-s in the presence of 0.5 and 2 M NaCl. Concentration profiles were monitored, with absorbance at 280 nm. Sedimentation velocity data were acquired at 50,000 rpm. The protein partial specific volumes, buffer densities, and viscosities at each NaCl concentration were calculated from the amino-acid sequence and buffer composition, using the program SEDNTERP (kindly provided by J. Philo, Alliance Protein Laboratories, Camarillo, CA). The data were analyzed with the program SEDFIT (http://www.analyticalultracentrifugation.com), which is based on direct modeling of the sedimentation boundary, using finite-element solutions of the Lamm equation. The obtained $c(s)$ was converted to $c(M)$, assuming that the value of the frictional ratio, ff_0, was common to all the molecular species.

CD measurements

Far-ultraviolet (UV) CD spectra of 0.2 mg/mL NDK-q and NDK-s were recorded on a J-720 spectropolarimeter (Jasco, Tokyo, Japan) at 25°C, using a 1-mm path length cell. Because the dynode voltage exceeded 0.6 kV below 205 nm due to the high NaCl concentration, the CD data were collected in a range of 205–260 nm at 0.2-nm intervals. The results were expressed as mean residue ellipticity (MRE) values. Helicity was calculated using the algorithm proposed by Chen et al. (19).

RESULTS

Structure determination

The crystal structure of N-terminal (6 × His)-tagged NDK-q was determined at 2.6-Å resolution by molecular replacement. The final structure included four protomers (residues 2–154 for chains A, C, and D, and residues 3–154 for chain B) and seven water molecules in the asymmetric unit. No electron density was evident for the remaining residues and N-terminal (6 × His)-tag. The Matthews coefficient (V_m) (20) was 2.07 Å^3/Da, and the estimated solvent content was 40.7%. In the Ramachandran plot, 91.7%, 7.2%, 0.6%, and 0.6% of the residues were located in the most favored regions, additionally allowed regions, generously allowed regions, and disallowed regions, respectively. The data collection and refinement statistics are summarized in Table 1. The NDK-q protomer contained four β-strands, eight α-helices, and three 3_{10}-helices (Fig. 1, *A* and *B*). Like the other NDKs, NDK-q exhibited a ferredoxin fold composed of $\beta1$-$\alpha2$-$\beta2$ and $\beta3$-$\alpha5$-$\beta4$, a Kpn loop (residues 96–117), and a C-terminal extension (residues 136–154). The active site of NDK-q was located at the edge of the β-sheet, and the nucleophile His^{118} was at the bottom of the active site. Arg^{31}, the only residue different from the residues of NDK-s, was located at the end of $\alpha2$.

The quaternary structure of NDK-q observed in the crystal was hexameric (Fig. 2 *A*). The four protomers in an asymmetric unit formed two dimers (AD and BC), which generated two hexamers (A_3D_3 and B_3C_3) by the symmetry operation around the threefold crystallographic symmetry axis. According to calculations using the PISA server (21), the buried area in the dimer interface (between protomers in the same asymmetric unit) was 1000 Å^2 (12% of the surface area of each protomer) with 14 hydrogen bonds, and the buried area in the trimer interface (between protomers of neighboring asymmetric units) was 840 Å^2 (10% of the surface area of each protomer) with 19 hydrogen bonds. Arg^{31} was located in the middle of the trimer interface, and interacted with main-chain oxygens of Pro^{96} and Gly^{109} in the Kpn loop.

TABLE 1 Summary of data collection and refinement statistics

Data collection	
Wavelength (Å)	1.0000
Resolution range (Å)	50.0–2.59 (2.68–2.59)
Number of observed reflections	659,596
Number of unique reflections	20,457
Data completeness (%)	95.7 (100.0)
R_{merge} [†]	0.084 (0.426)
$\langle I\rangle/\langle\sigma(I)\rangle$	30.7 (4.2)
Space group	$P6_3$
Unit cell parameters	A = B = 73.57 Å, C = 214.27 Å
Refinement	
Resolution range used for refinement (Å)	50.0–2.59
R_{factor} (%)[‡]	22.2
R_{free} (%)[‡]	28.9
Number of reflections used for refinement	18,544
Protein residues modeled	611 OF 696
Number of protein atoms modeled	4894
Number of water molecules modeled	7
Mean overall B value (Å^2)	47.0
RMSD bond angles (°)	1.238
RMSD bond length (Å)	0.009
Ramachandran plot	
Residues in most favored regions (%)	91.7
Residues in additionally allowed regions (%)	7.2
Residues in generously allowed regions (%)	0.6
Residues in disallowed regions (%)	0.6

*Values in parentheses are for highest-resolution shell.
[†]$R_{\text{merge}} = \Sigma_{hkl}\,[(\Sigma_i|I_i - \langle I\rangle|)/\Sigma_i|I_i|]$.
[‡]$R_{\text{factor}} = (\Sigma_{hkl}||F_o| - |F_c||)/\Sigma_{hkl}|F_o|$. R_{free} was calculated with 5% of data excluded from refinement.
RMSD, root mean-square deviation.

Structural comparison with other NDKs

A structural-similarity search was performed with the atomic coordinates of NDK-q, using the DALI server (22). The top five results involved NDKs from *H. salinarum* (81% identical in amino-acid sequence; PDB code 2AZ3) (7), *Pisum sativum* (51% identical; PDB code 1W7W) (23), *Drosophila melanogaster* (52% identical; PDB code 1NSQ) (24), and two NDKs from humans (54% identical, PDB code 1JXV; and 51% identical, PDB code 1ZS6) (25). They all exist as hexamers in a crystal, and the root mean-square deviations between corresponding C^α atoms of NDK-q and 2AZ3, 1W7W, 1NSQ, 1JXV, and 1ZS6 are 0.9 Å for 151 C^α, 0.7 Å for 150 C^α, 0.7 Å for 149 C^α, 0.7 Å for 148 C^α, and 0.9 Å for 150 C^α, respectively. Both NDK-q and a halobacterial NDK (2AZ3) have exposed molecular surfaces, with highly negative charges (Fig. 2 *B*). Their superposition indicates

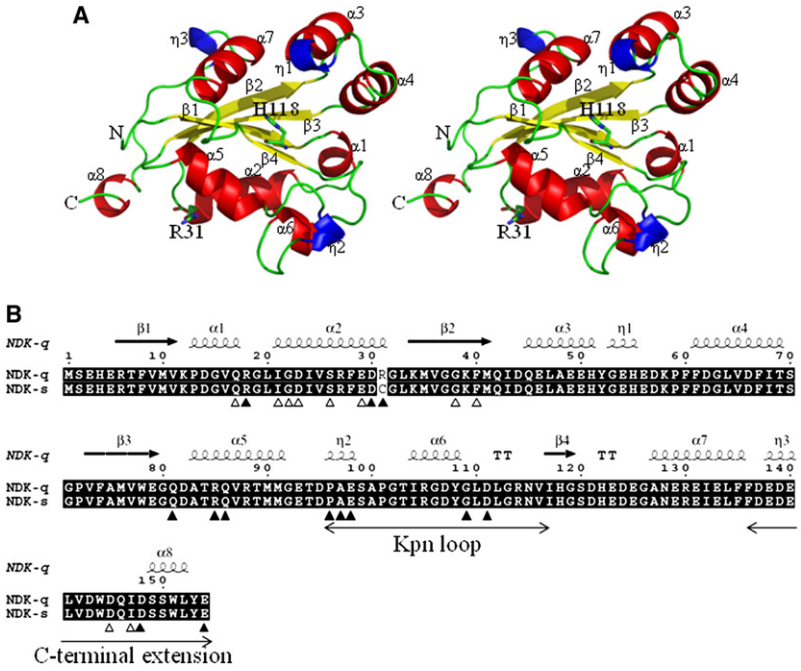

FIGURE 1 (*A*) Stereo view of NDK-q protomer's overall structure. The N-termini and C-termini are labeled N and C, respectively. The β-strands (β1–4), α-helices (α1–8), and 3_{10}-helices (η1–3) are shown in yellow, red, and blue, respectively. His^{118}, a putative catalytic residue, and Arg^{31}, the only residue distinct from those in NDK-s, are shown as a stick diagram. Images were created using PyMOL (30). (*B*) Amino-acid sequence alignment of NDK-q and NDK-s. Secondary structure elements are shown above alignment. Residues involved in interactions of dimeric and trimeric interfaces are indicated by white and black arrowheads, respectively. Graphics were created using ESPript (31).

that their cytidine diphosphate (CDP)-binding residues are completely conserved, which suggests that NDK-q binds its substrate in the same manner as 2AZ3 (Fig. 2 *C*).

Oligomeric state analyses

Analytical ultracentrifugation analyses (sedimentation velocity experiments) of NDK-q and NDK-s in solutions containing 0.5 and 2 M NaCl were performed to analyze their oligomeric states. The results indicate that NDK-q (19.7 kDa in monomer) was present as a hexamer in both 0.5 and 2 M NaCl (114 and 104 kDa, respectively), and that NDK-s (19.7 kDa in monomer) was present as a hexamer in 2 M NaCl (111 kDa), and as a dimer in 0.5 M NaCl (42 kDa) (Table 2). In addition, gel-filtration analyses of NDK-q and NDK-s were performed with a Superdex 200 HR 10/30 column (GE Healthcare Biosciences) in solutions containing 0.2, 0.5, 1, 2, 3, and 4 M NaCl to analyze their oligomeric states at various NaCl concentrations (see Fig. S1 in the Supporting Material). When 100 μL of 1 mg/mL NDK-q and NDK-s solutions were injected, NDK-q at all NaCl concentrations and NDK-s at NaCl concentrations above 1 M showed elution volumes of 13.0–14.2 mL, whereas NDK-s at NaCl concentrations below 1 M showed elution volumes of 14.7–15.0 mL, suggesting that the former and latter peaks corresponded to hexamers and dimers, respectively. It should be noted that NDK-s existed as a mixture of dimers and hexamers in the presence of 1 M NaCl. The results indicate that hexameric NDK-s dissociates into dimers at low salt concentrations below 1 M NaCl, whereas NDK-q maintained its hexameric assembly at all salt concentrations tested (0.2–4 M NaCl). The different oligomerization behaviors of NDK-q and NDK-s at low NaCl concentrations must be attributable to the difference at the thirty-first position in their amino-acid sequence, i.e., Arg^{31} in NDK-q and Cys^{31} in NDK-s. To examine the effect of protein concentration on its oligomeric state, NDK-s was subjected to gel-filtration analysis at two concentrations (1 and 0.2 mg/mL). At 2 M NaCl, no dissociation to the dimeric configuration was detected at either of the two NDK-s concentrations. At 1 M NaCl, the dimer-to-hexamer ratios of NDK-s were 2.3:1 and 5.7:1 when 1 and 0.2 mg/mL proteins were loaded onto the column, respectively, indicating that dissociation depended on NDK-s concentration. Thus, hexameric NDK-s was stable at high NaCl concentrations above 2 M, and was destabilized and dissociated into dimers at low NaCl concentrations below 1 M.

CD analyses

The CD spectra of NDK-q and NDK-s in 0.2, 0.5, 1, 2, 3, and 4 M NaCl were recorded to analyze the effect of NaCl concentration on secondary structure. NDK-q and NDK-s exhibited two distinct spectral patterns: one for NDK-q at all NaCl concentrations tested and NDK-s at high NaCl concentrations (above 2 M), and the other for NDK-s at low NaCl concentrations (below 1 M) (Fig. 3 *A*). The CD analyses indicated that the secondary structure of NDK-q was not affected by salt concentration in a range of 0.2–4 M NaCl, whereas the secondary structure of NDK-s was affected by the salt concentration. The secondary structures of NDK-q and NDK-s were almost identical at high NaCl concentrations (above 2 M), but the secondary structure of NDK-s changed remarkably at low NaCl concentrations (below 1 M). The MRE at 222 nm of NDK-s was $\sim -8500^\circ \cdot \mathrm{cm}^2 \cdot \mathrm{dmol}^{-1}$ at high NaCl concentrations (above 2 M), and $\sim -9500^\circ \cdot \mathrm{cm}^2 \cdot \mathrm{dmol}^{-1}$ at low NaCl concentrations (below 1 M). Because hexameric and

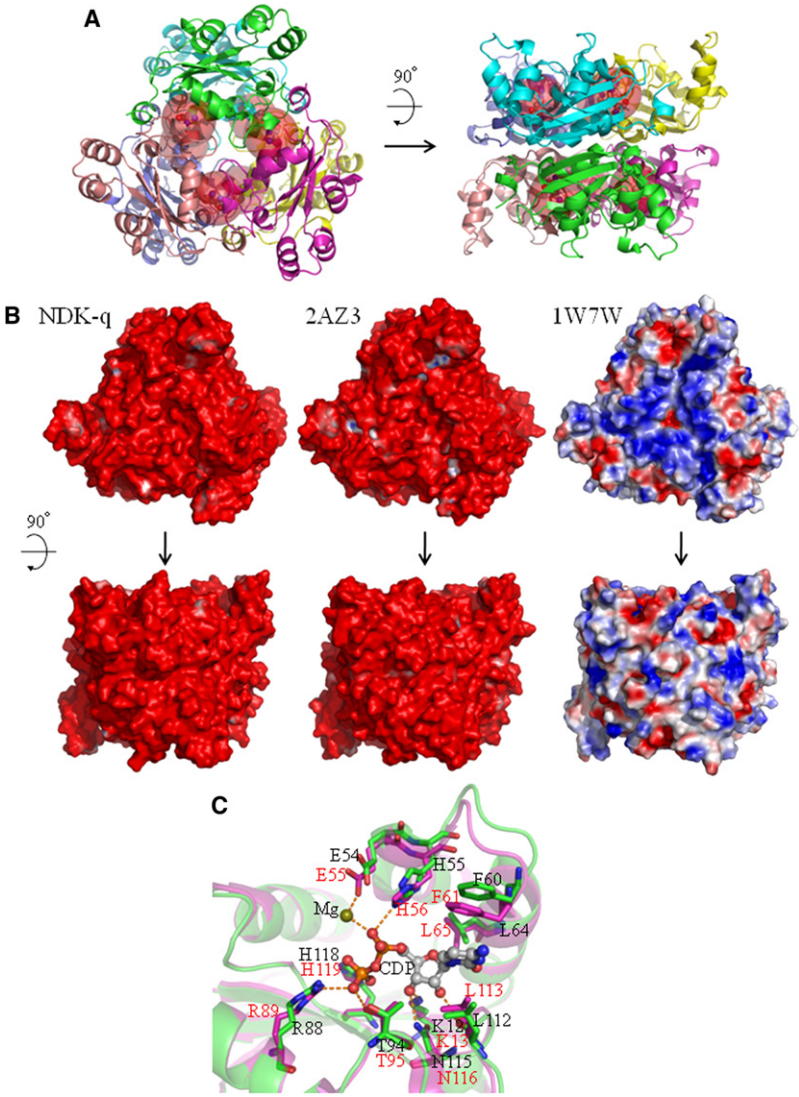

FIGURE 2 (*A*) Hexameric structure (A_3D_3) of NDK-q, viewed along threefold (*left*) and twofold (*right*) axes. Trimeric chains A are shown in green, magenta, and pink, and chains D are shown in cyan, yellow, and light blue. Arg^{31}, shown as a ball and stick model and highlighted by red spheres, is located in middle of trimer interface. (*B*) Electrostatic surface presentation of NDK-q (*left*), 2AZ3 (*center*), and 1W7W (*right*), viewed along threefold (*up*) and twofold (*down*) axes. Electrostatic potentials, calculated by APBS (32), are indicated as color gradient from red ($-15k_BT$) to blue ($15k_BT$). (*C*) Superposed diagram of substrate-binding sites of NDK-q (*green*) and 2AZ3 (*magenta*). The CDP molecule in 2AZ3 coordinate file is shown as a ball-and-stick model. Residues involved in CDP recognition are shown as a stick diagram. Residue numbers for NDK-q and 2AZ3 are shown in black and red, respectively. Images were created using PyMOL (30).

dimeric NDK-s were separable in 2 M NaCl, we compared their CD spectra. The CD spectra of hexameric and dimeric NDK-s were different from each other in 2 M NaCl (Fig. 3 *B*). The CD data suggest that the dissociation of hexamers to dimers increased helicity by ~20%. The CD spectrum of dimeric NDK-s in 2 M NaCl was identical to that of NDK-s (a mixture of hexameric and dimeric forms) at NaCl concentrations below 1 M. Thus the CD spectra as well as gel-filtration chromatograms indicate that NDK-s was mostly present as a dimer under low NaCl conditions.

NDK activity assay

Activity assays of NDK-q and NDK-s were performed by using the coupled assay of ADP phosphorylation and the luciferin-luciferase reaction. The activity of NDK-q in 1 M NaCl was defined as 100%, and the relative activity was plotted against NaCl concentration (Fig. 4). The results demonstrated that optimal NaCl concentrations of NDK-q and NDK-s were 1 and 2 M, respectively. At NaCl concentrations above 2 M, NDK-s showed ~50% of the activity of NDK-q. However, the activity of NDK-s fell significantly at NaCl concentrations below 1 M. In contrast, NDK-q exhibited its highest activity in 1 M NaCl, and retained ~80% of its activity in 0 M NaCl. At NaCl concentrations above 2 M, NDK-s was mainly present as a hexamer, and was twice as active as dimeric NDK-s. However, at NaCl concentrations below 1 M, their activities were almost the same. Therefore, the decrease in NDK-s activity at NaCl concentrations below 1 M was caused by the dissociation of hexamers to dimers. The optimal NaCl concentration for dimeric NDK-s was 1 M. Fig. 5 summarizes the salt dependencies of the oligomeric states and activities of NDK-q and NDK-s. In 4 M NaCl, the optimal NaCl concentration for the growth of the haloarchaea NDK-q and NDK-s retained 35% and 49%, respectively, of their optimal activity.

TABLE 2 Molecular masses determined by sedimentation velocity

	[NaCl] (M)	Sedimentation coefficient (S)	Molecular mass (kDa)
NDK-Q	0.5	1.30	114
	2.0	1.30	104
NDK-S	0.5	0.46	42
	2.0	1.35	111

DISCUSSION

Two NDKs from *H. quadrata* and *H. sinaiiensis*, NDK-q and NDK-s, respectively, differ only at the thirty-first position, i.e., Arg^{31} for NDK-q and Cys^{31} for NDK-s. In almost all archaeal and eukaryal NDKs, the corresponding position is occupied by Arg or Lys, whereas in bacterial NDKs, it is occupied by Lys or Ala. In this sense, the Cys at this position is quite unusual. The different residues at this position result in different optimal NaCl concentrations (10). To investigate the structural basis for the different salt-dependent activity profiles of NDK-q and NDK-s, the crystal structure of hexameric NDK-q was used to build a homology-based model of hexameric NDK-s. The replacement of Arg^{31} in NDK-q to Cys was performed using the program Coot (26).

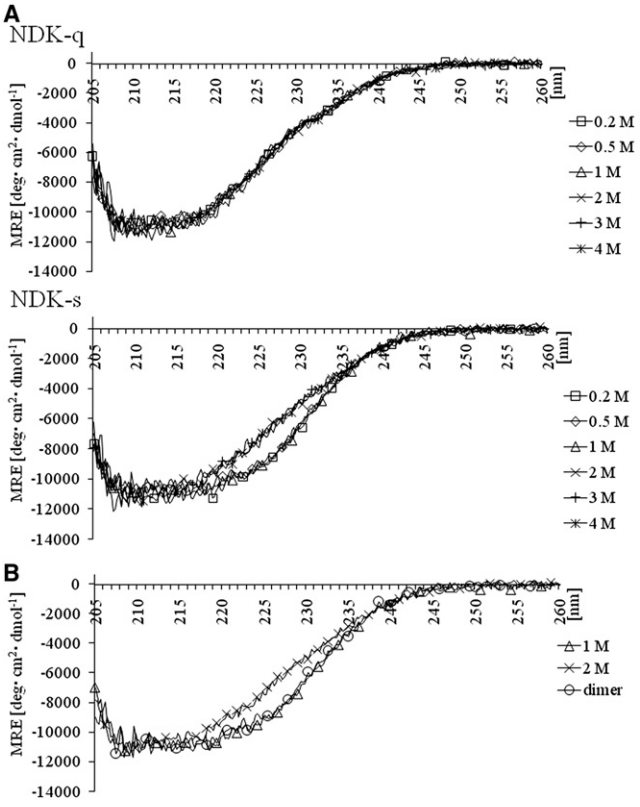

FIGURE 3 (*A*) Far-UV CD spectra of NDK-q (*up*) and NDK-s (*down*) in 0.2, 0.5, 1, 2, 3, and 4 M NaCl. (*B*) Far-UV CD spectra of dimeric NDK-s in 2 M NaCl, along with those of normally prepared NDK-s in 1 and 2 M NaCl. The MRE is plotted against the wavelength.

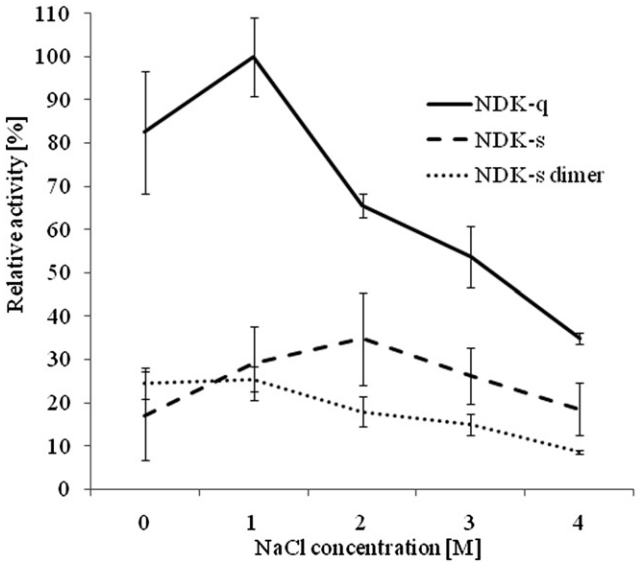

FIGURE 4 Relative activities of NDK-q, NDK-s, and NDK-s dimer at various NaCl concentrations. Maximum activity of NDK-q (at 1 M NaCl) is defined as 100%. Error bars represent standard deviation from mean of three trials.

Structural insights into distinct salt-dependent quaternary-structure transitions between NDK-q and NDK-s

Hexameric NDK-q is stable under a wide range of NaCl concentrations (0.2–4 M), whereas hexameric NDK-s is less stable and thus dissociates into dimers at NaCl

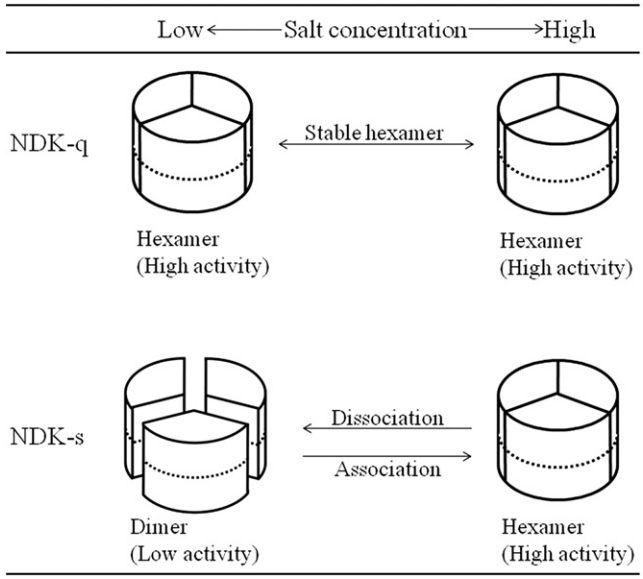

FIGURE 5 Schematic model of salt dependencies of oligomeric states and activities of NDK-q and NDK-s. Trimeric and dimeric interfaces are shown as solid and dotted lines, respectively. NDK-q is stable as a highly active hexamer under a wide range of NaCl concentrations (0.2–4 M). On the other hand, the highly active hexamer of NDK-s dissociates into less active dimers at low salt concentrations (below 1 M NaCl).

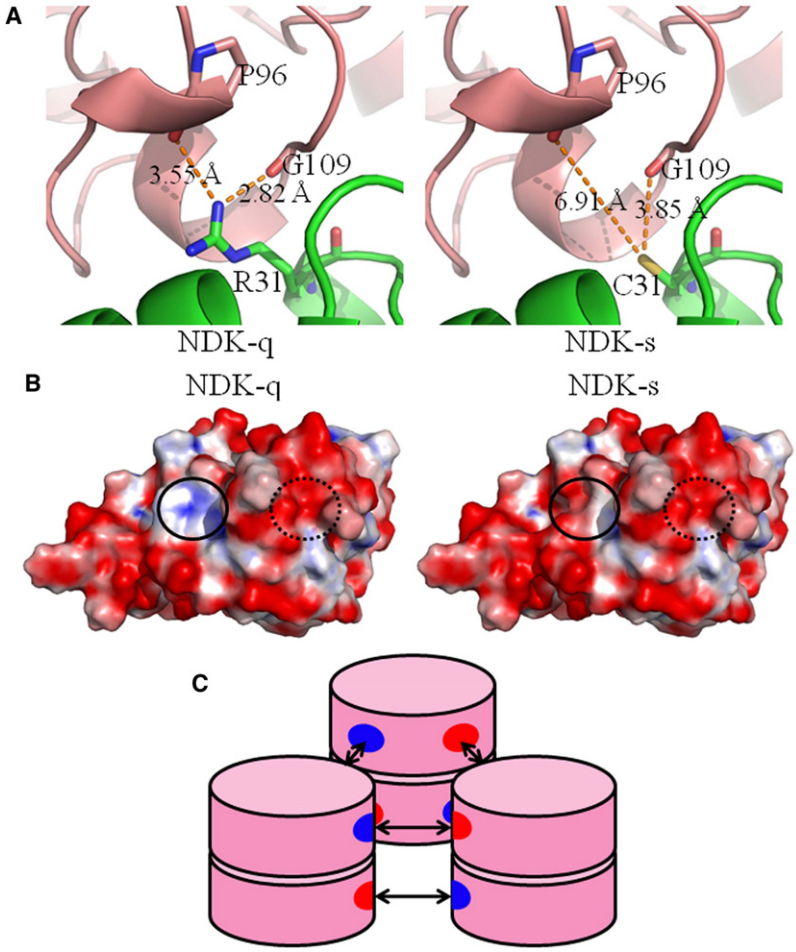

FIGURE 6 (*A*) Comparison of distances between Arg^{31} of NDK-q (*left*) or Cys^{31} of NDK-s (*right*) and main-chain oxygens of Pro^{96} and Gly^{109} of neighboring subunit. Two neighboring subunits are shown in green and pink. (*B*) Electrostatic surface presentation of protomer of NDK-q (*left*) and NDK-s (*right*) facing the thirty-first residue. Electrostatic potentials, calculated by APBS (32), are indicated as a color gradient from red ($-15k_BT$) to blue ($15k_BT$). The thirty-first residues are indicated by circles, and counterparts of the thirty-first residue in hexameric coordination are indicated by dotted circles. (*C*) Schematic model of formation of hexameric NDK-q. Arg^{31} and its counterparts are shown in red and blue, respectively. Images were created using PyMOL (30).

concentrations below 1 M. In hexameric NDK-q, $N^{\eta 1}$ of Arg^{31} makes hydrogen bonds with the backbone oxygens of Pro^{96} and Gly^{109} in the Kpn loop (Fig. 6 *A*). Moreover, Arg^{31} creates a positively charged surface in the center of the trimer interface that interacts with its negatively charged counterpart (Fig. 6, *B* and *C*). These preferable interactions are lost in NDK-s (Fig. 6, *A* and *B*). Therefore, NDK-s was dissociated into dimers by electrostatic repulsion at low salt concentrations. At high salt concentrations, the salt cations (Na^+) shield the electrostatic repulsion between negatively charged surfaces. A similar but reverse phenomenon was previously reported, i.e., that the dimer/monomer ratio of β-lactoglobulin at pH 3 increases at high salt concentrations, because the salt anions (Cl^-) shield the electrostatic repulsion between positively charged surfaces that otherwise promote the dissociation (27). In NDK-s, the bulky sulfur atom of Cys^{31} might destabilize the hexamer by disrupting the packing of the trimer interface. However, the thiol group of Cys^{31} does not have van der Waals contacts with other residues in the neighboring subunit in the NDK-s model, and thus the contribution of the bulkiness of the sulfur atom to the dissociation of NDK-s into dimers should be weaker than that of electrostatic repulsion.

Interaction between Arg^{31} and the Kpn loop stabilizes the highly active conformation

When we compared the hexameric forms of NDK-q and NDK-s in 2 M NaCl, the former exhibited twice as much activity as the latter, although their CD spectra were almost identical. The only different residues, Arg^{31} of NDK-q and Cys^{31} of NDK-s, are far from the active sites that are located outside the hexameric assembly. However, Arg^{31} interacts with the Kpn loop of the neighboring subunit. The Kpn loop includes substrate-binding residues, and its flexibility lowers NDK activity (28). Because the interaction of Arg^{31} with the Kpn loop is stronger than that of Cys^{31} (Fig. 6 *B*), the Kpn loop in hexameric NDK-q should be less flexible than in hexameric NDK-s, resulting in the difference in NDK activity between the hexameric forms of NDK-q and NDK-s. We also revealed that the dissociation of hexameric NDK-s into dimers at NaCl concentrations below 1 M affects its activity. The optimal NaCl concentrations of NDK-q and NDK-s are therefore different. The CD spectra of the hexameric and dimeric forms of NDK-s are remarkably different: the helicity of NDK-s increases by ~20% when hexameric NDK-s dissociates into dimers. When hexameric NDK-s dissociates into dimers, the interaction between the Kpn loop and the

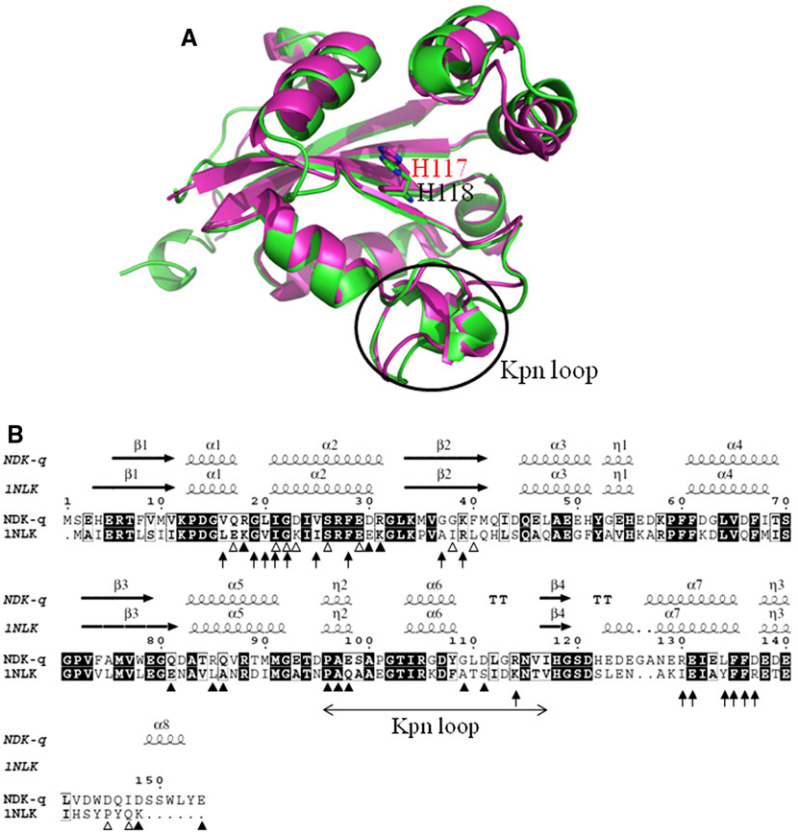

FIGURE 7 (*A*) Superposed diagram of NDK-q (*green*) and 1NLK (*magenta*). Catalytic His residues are shown as a stick diagram. Residue numbers for NDK-q and 1NLK are shown in black and red, respectively. Kpn loops are indicated by circles. Images were created using PyMOL (30). (*B*) Amino-acid sequence alignment of NDK-q and 1NLK. Secondary structure elements of NDK-q and 1NLK are shown above alignment. Residues involved in interactions of dimeric and trimeric interfaces of NDK-q are indicated by white and black arrowheads, respectively, and tetrameric interfaces of 1NLK are indicated by black arrows. Graphics were generated by ESPript (31).

neighboring subunit disappears, and as a result, the Kpn loop would form helices in the absence of conformational restraints, resulting in a decrease in activity. This phenomenon is different from the case of *H. salinarum* NDK, where the helicity decreases when hexameric *H. salinarum* NDK dissociates into dimers at low salt concentrations (8).

Interestingly, *Myxococcus xanthus* NDK (43% identical to NDK-q; PDB code 1NLK) (29), a tetrameric NDK with known structure, does not exhibit any interaction between the Kpn loop and the neighboring subunit. However, a comparison of protomer structures between hexameric NDK-q and tetrameric *Myxococcus xanthus* NDK (PDB code 1NKL) revealed that the overall structures of these protomers are almost identical, including the Kpn loops, with an root mean-square deviation of 1.3 Å for 143 C^{α} (Fig. 7 *A*). The sequence comparison of the Kpn loops of NDK-q and 1NKL revealed that residues 96–108 and 114–117 are conserved, but residues 109–113 are different: GLDLG in NDK-q, and ATSID in 1NLK (Fig. 7 *B*). The GLDLG segment of NDK-q interacts with Arg^{31} and Glu^{154} of the neighboring subunit, and requires the interaction to maintain its conformation. On the other hand, the ATSID segment of 1NLK will adopt a more rigid conformation on its own.

CONCLUSIONS

We revealed the structural basis of the different salt-dependent activity profiles of NDK-q and NDK-s. In NDK-q, Arg^{31} contributes to the stabilization of the hexameric assembly under a wide range of salt concentrations (0.2–4 M NaCl). On the other hand, in NDK-s, the highly active hexamer dissociates into less active dimers at low salt concentrations (below 1 M NaCl). Hexameric NDK-s is more active than the dimer, because the Kpn loop is more restrained in the hexamer than in the dimer. The dissociation of NDK-s at low salt concentration lowers its activity, leading to the different salt-dependent activity profiles of NDK-q and NDK-s. In 4 M NaCl, the optimal NaCl concentration for the growth of these haloarchaea, NDK-q and NDK-s retained 35% and 49%, respectively, of their optimal activity. Because the remaining activities of NDK-q and NDK-s at 4 M NaCl sufficed for the growth of *H. quadrata* and *H. sinaiiensis*, respectively, the mutation from Arg to Cys at position 31 did not act as a selection pressure during the evolution of haloarchaeal NDKs.

SUPPORTING MATERIAL

One figure is available at http://www.biophysj.org/biophysj/supplemental/S0006-3495(09)00747-4.

The synchrotron-radiation experiments were performed at beamline NW12 at Photon Factory-Advanced Ring (Tsukuba, Japan), with the approval of the Photon Factory, High Energy Accelerator Research Organization (Proposal 2006S2-006).

This work was supported by the National Project on Protein Structural and Functional Analyses, and by the Targeted Proteins Research Program, of the Ministry of Education, Culture, Sports, Science, and Technology of Japan.

REFERENCES

1. Bernard, M. A., N. B. Ray, M. C. Olcott, S. P. Hendricks, and C. K. Mathews. 2000. Metabolic functions of microbial nucleoside diphosphate kinases. *J. Bioenerg. Biomembr.* 32:259–267.
2. Janin, J., C. Dumas, S. Moréra, Y. Xu, P. Meyer, et al. 2000. Three-dimensional structure of nucleoside diphosphate kinase. *J. Bioenerg. Biomembr.* 32:215–225.
3. Lascu, L., A. Giartosio, S. Ransac, and M. Erent. 2000. Quaternary structure of nucleoside diphosphate kinases. *J. Bioenerg. Biomembr.* 32:227–236.
4. Madern, D., C. Ebel, and G. Zaccai. 2000. Halophilic adaptation of enzymes. *Extremophiles.* 4:91–98.
5. Mevarech, M., F. Frolow, and L. M. Gloss. 2000. Halophilic enzymes: proteins with a grain of salt. *Biophys. Chem.* 86:155–164.
6. Polosina, Y. Y., K. F. Jarrell, O. V. Fedorov, and A. S. Kostyukova. 2000. Nucleoside diphosphate kinase from haloalkaliphilic archaeon *Natronobacterium magadii*: purification and characterization. *Extremophiles.* 2:333–338.
7. Besir, H., K. Zeth, A. Bracher, U. Heider, M. Ishibashi, et al. 2005. Structure of a halophilic nucleoside diphosphate kinase from Halobacterium salinarum. *FEBS Lett.* 579:6595–6600.
8. Ishibashi, M., T. Arakawa, J. S. Philo, K. Sakashita, Y. Yonezawa, et al. 2002. Secondary and quaternary structural transition of the halophilic archaeon nucleoside diphosphate kinase under high- and low-salt conditions. *FEMS Microbiol. Lett.* 216:235–241.
9. Ishibashi, M., S. Tatsuda, K. Izutsu, K. Kumeda, T. Arakawa, et al. 2007. A single Gly114Arg mutation stabilizes the hexameric subunit assembly and changes the substrate specificity of halo-archaeal nucleoside diphosphate kinase. *FEBS Lett.* 581:4073–4079.
10. Mizuki, T., M. Kamekura, M. Ishibashi, R. Usami, Y. Yoshida, et al. 2004. Nucleoside diphosphate kinase of halobacteria. Amino acid sequence and salt-response pattern. *J. Jap. Soc. Extremophiles.* 3: 18–27.
11. Otwinowski, Z., and W. Minor. 1997. Processing of x-ray diffraction collected in oscillation mode. *Methods Enzymol.* 276:307–326.
12. Collaborative Computational Project, Number 4. 1994. The CCP4 suite: programs for protein crystallography. *Acta Crystallogr. D Biol. Crystallogr.* 50:760–763.
13. Vagin, A., and A. Teplyakov. 2000. An approach to multi-copy search in molecular replacement. *Acta Crystallogr. D Biol. Crystallogr.* 56:1622–1624.
14. McRee, D. E. 1999. XtalView/Xfit.–A versatile program for manipulating atomic coordinates and electron density. *J. Struct. Biol.* 125:156–165.
15. Brunger, A. T., P. D. Adams, G. M. Clore, W. L. DeLano, P. Gros, et al. 1998. Crystallography and NMR system: a new software suite for macromolecular structure determination. *Acta Crystallogr. D Biol. Crystallogr.* 54:905–921.
16. Murshudov, G. N., A. A. Vagin, and E. J. Dodson. 1997. Refinement of macromolecular structures by the maximum-likelihood method. *Acta Crystallogr. D Biol. Crystallogr.* 53:240–255.
17. Laskowski, R. A., M. W. MacArthur, D. S. Moss, and J. M. Thornton. 1993. PROCHECK: a program to check the stereochemistry quality of protein structures. *J. Appl. Cryst.* 26:283–291.
18. Holm, L., and J. Park. 2000. DaliLite workbench for protein structure comparison. *Bioinformatics.* 16:566–567.
19. Chen, Y. H., J. T. Yang, and H. Martinez. 1972. Determination of the secondary structures of proteins by circular dichroism and optical rotatory dispersion. *Biochemistry.* 11:4120–4131.
20. Matthews, B. W. 1968. Solvent content of protein crystals. *J. Mol. Biol.* 33:491–497.
21. Krissinel, E., and K. Henrick. 2005. Detection of protein assemblies in crystals. *In* CompLife 2005, LNBI 3695. M. R. Berthold, R. Glen, K. Diederichs, O. Kohlbacher, and I. Fischer, editors. Springer-Verlag, Berlin. 163–174.
22. Holm, L., and C. Sander. 1995. DALI: a network tool for protein structure comparison. *Trends Biochem. Sci.* 20:478–480.
23. Johansson, M., A. Mackenzie-Hose, I. Andersson, and C. Knorpp. 2004. Structure and mutational analysis of a plant mitochondrial nucleoside diphosphate kinase. Identification of residues involved in serine phosphorylation and oligomerization. *Plant Physiol.* 136:3034–3042.
24. Morera, S., M. Chiadmi, G. LeBras, I. Lascu, and J. Janin. 1995. Mechanism of phosphate transfer by nucleoside diphosphate kinase: x-ray structures of the phosphohistidine intermediate of the enzymes from *Drosophila* and *Dictyostelium*. *Biochemistry.* 34:11062–11070.
25. Min, K., H. K. Song, C. Chang, S. Y. Kim, K. J. Lee, et al. 2002. Crystal structure of human nucleoside diphosphate kinase A, a metastasis suppressor. *Proteins.* 46:340–342.
26. Emsley, P., and K. Cowtan. 2004. Coot: model-building tools for molecular graphics. *Acta Crystallogr. D Biol. Crystallogr.* 60:2126–2132.
27. Sakurai, K., M. Oobatake, and Y. Goto. 2001. Salt-dependent monomer-dimer equilibrium of bovine beta-lactoglobulin at pH 3. *Protein Sci.* 10:2325–2335.
28. Karlsson, A., S. Mesnildrey, Y. Xu, S. Moréra, J. Janin, et al. 1996. Nucleoside diphosphate kinase. Investigation of the intersubunit contacts by site-directed mutagenesis and crystallography. *J. Biol. Chem.* 271:19928–19934.
29. Williams, R. L., D. A. Oren, J. Munoz-Dorado, S. Inouye, M. Inouye, et al. 1993. Crystal structure of *Myxococcus xanthus* nucleoside diphosphate kinase and its interaction with a nucleotide substrate at 2.0 Å resolution. *J. Mol. Biol.* 234:1230–1247.
30. DeLano, W. L. 2002. The PyMOL Molecular Graphics System. DeLano Scientific, Palo Alto, CA.
31. Gouet, P., E. Courcelle, D. I. Stuart, and F. Metoz. 1999. ESPript: analysis of multiple sequence alignments in PostScript. *Bioinformatics.* 15:305–308.
32. Baker, N. A., D. Sept, S. Joseph, M. J. Holst, and J. A. McCammon. 2001. Electrostatics of nanosystems: application to microtubules and the ribosome. *Proc. Natl. Acad. Sci. USA.* 98:10037–10041.